JAAS
Journal of Analytical Atomic Spectrometry

Accepted Manuscript

This article can be cited before page numbers have been issued, to do this please use: Z. Weiss, V. Smola, M. Lebeda, P. Vlcak, J. Lorincik, I. Elantyev and P. Malinský, *J. Anal. At. Spectrom.*, 2026, DOI: 10.1039/D6JA00037A.

Analysis of nitrogen implantation profiles in titanium and Ti-Nb alloys by glow discharge optical emission spectroscopy: nitrogen calibration[1]

Zdeněk Weiss[a], Vojtěch Smola[b], Miroslav Lebeda[b,c], Petr Vlčák[b], Jan Lorinčík[d], Ivan Elantyev[d], Petr Malinský[e,f]

a: FZU - Institute of Physics of the Czech Academy of Sciences, Na Slovance 2, 182 00 Prague, Czech Republic

b: Department of Physics, Faculty of Mechanical Engineering, Czech Technical University in Prague, Technicka 4, 16607 Prague, Czech Republic

c: Department of Solid State Engineering, Faculty of Nuclear Sciences and Physical Engineering, Czech Technical University in Prague, Trojanova 339/13, 12000 Prague, Czech Republic

d: Research Centre Řež, 250 68 Husinec-Řež, Czech Republic

e: Nuclear Physics Institute, AS CR, 250 68 Řež, Czech Republic

f: Department of Physics, Faculty of Science, University of J. E. Purkyně, Pasteurova 3632/15, 400 96 Ústí nad Labem, Czech Republic

Abstract

In the analysis of nitrogen in Ti-based matrices by glow discharge emission spetroscopy (GDOES), emission yield of the N I 149.262 nm line was found to depend on the sample composition, in particular, on the N/Ti ratio of the sample surface being sputtered. This was attributed to differences in the transport and redeposition of nitrogen in the GDOES discharge cell: if the surfaces surrounding the plasma consist largely of elemental Ti, the sticking coefficient of nitrogen on them is high and the number density of nitrogen in the volume of the plasma is reduced by adsorption more strongly than if these surfaces are partly or completely saturated with nitrogen. This leads to a decrease of emission yields of nitrogen lines and needs to be reflected in the analytical methodology. Analogous mechanism might be at play in the analysis of other gaseous elements also.

[1]presented at the 7th International Glow Discharge Spectroscopy Symposium (7th IGDSS), 19-22 April 2026, Antwerp, Belgium

View Article Online
DOI: 10.1039/D6JA00037A

Introduction

Analysis of nitrogen in nitride coatings and nitrogen-enriched surface layers of some metals is a frequent task, reflecting the importance of such materials in science and technology. Important is the Ti-N system, and, in a broader perspective, various complex coatings in which titanium and nitrogen are present at high concentrations, see e.g. [1, 2]. Different methods were considered for the analysis of the Ti-N stoichiometry and attempts have been under way to develop the corresponding methodology for a long time [3]. They involve energy- and wavelength dispersive electron microanalysis (EDS, WDS) [4,5], electron spectroscopies [6-10], accelerator-based methods [11,12], secondary-ion mass spectrometry (SIMS) [13] and glow-discharge optical emission spectroscopy (GDOES) [8, 14-19]. The most common method of these, EDS/WDS, typically available in scanning electron microscopes, suffers from an overlap of titanium L- and nitrogen K-peaks [5] and the same problem occurs in Auger electron spectroscopy: overlap of the Ti – $L_3M_{23}N_{23}$ (383 eV) and N – $KL_{23}L_{23}$ (381 eV) signals [7]. This makes the Ti-N analyses by these methods difficult. Moreover, EDS/WDS cannot be used for analysis of ion-implanted materials because the thereby produced depth distributions are too shallow. Therefore, GDOES is a viable alternative for such materials.

GDOES is a relative method relying on calibration by bulk reference materials (RMs) with known compositions and sputter rates. For nitrogen calibrations, a popular class of such materials are the 'Nitronic'-type stainless steels alloyed with nitrogen, for which good commercially available RMs are available, with nitrogen content up to ≈ 0.9 wt.% N. For higher nitrogen concentrations, there is only one RM, a special cutting material called Coronite (JK 41-1N, the SWERIM Metals Res. Inst., Stockholm) with 6.9 wt.% N, the composition of which corresponds to titanium nitride mixed with a high-speed steel with an addition of cobalt. In Ref. [16], describing the comparison of GDOES and the Rutherford backscattering spectroscopy (RBS) in the analysis of CrN_x coatings, a TiN coating with a stoichiometry claimed to be 1:1 (non-certified, ≈ 23 wt.% N) was used as the high point in an essentially two-point linear nitrogen calibration, consisting of a bunch of points with low concentrations of nitrogen, below ≈ 0.6 wt. %, and the TiN sample, with nothing in between. However, not even this yields a universal solution, as it follows from the analyses described below. The main goal of this note is to describe GDOES analyses of N-implanted titanium and TiNb alloys and offer a plausible explanation of the nitrogen signal response in these matrices, with some consequences for the GDOES methodology.

Experimental

A set of Ti, Ti-25%Nb, Ti-55%Nb samples, ion implanted with nitrogen, were analysed by GDOES depth profiling. Their designations reflect the composition of the base material and the declared nitrogen fluence, e.g., Ti25Nb_3E17N means titanium with 25 wt.% Nb, implanted by the fluence of 3.0×10^{17} atoms of nitrogen per square centimeter. The Ti-Nb materials were prepared by powder metallurgy. Details of the metallurgical fabrication of TiNb alloys are described in our previous work [10]. Prior to ion implantation, the samples were mechanically ground and polished to a mirror like finish.

Nitrogen implantation was performed using the Tecvac 221 Ion Implanter [19]. Nitrogen ions were implanted at an accelerating voltage of 90 kV. The ion beam current I_i was measured

View Article Online
DOI: 10.1039/D6JA00037A

by Faraday cup. The ion distribution in the ion beam was 15% for atomic ions and 85% for molecular ions (measured by mass spectrometry by Tecvac Ltd. company [20]). The total charge of ions, *Q,* was determined by integrating the ion current values using the trapezoidal method. The fluence of implanted nitrogen I_F (i.e. the number of nitrogen atoms implanted during the implantation period per area unit) was determined according to the relation:

$$I_F = \frac{Qk_t k_A}{Sq}, \quad (1)$$

where k_t is the tooling factor (the distance ratio between the Faraday cup and the sample position from the ion source, k_t=0.97), k_A expresses the abundance of nitrogen atoms implanted into the titanium target (k_A=7/4), *S* is the area of Faraday cup (0.86 cm^2) and *q* is the elementary charge (q=1.602·10^{-19} C).

GDOES analyses were made using the GDA750HR spectrometer (Spectruma Analytik GmbH, Germany). The emission lines used were Ti I 399.864 nm, Nb II 316.340 nm, N I 149.262 nm. Besides these elements, also carbon and hydrogen were analysed, by the lines C I 165.701 nm and H I 121.467 nm, respectively. The measurements were done with a 2.5 mm - internal diameter anode, in a dc discharge in argon, at 850 V, 15 mA. This corresponds to the working pressure of few hPa. Sputter rate-corrected calibrations [15, 21] were established for the elements under study. In this approach, the intensity $I_{\lambda(E),M}$ of a line $\lambda(E)$ of element *E* in the matrix (sample) *M* is supposed to follow the relation

$$I_{\lambda(E),M} = R_{\lambda(E)} c_{E,M} q_M + b_{\lambda(E)} \quad (2)$$

where $c_{E,M}$ is the concentration of element *E* in the matrix *M*, q_M is the sputter rate of that matrix, and $R_{\lambda(E)}$, $b_{\lambda(E)}$ are calibration constants, the former is called the *emission yield* of the line $\lambda(E)$, and the latter is the background intensity at the wavelength $\lambda(E)$. The resulting calibration functions of Ti, Nb and N are shown in Fig 1[2]. Unlike the other lines, the titanium line used here exhibits a non-linear intensity response as function of (*c.q*), as discussed, e.g., in Ref. [22]. Eqn (2) would not describe its response correctly and a quadratic approximation with an additional calibration parameter, $a_{\lambda(Ti)}$, was used instead:

$$a_{\lambda(Ti)} I^2_{\lambda(Ti),M} + I_{\lambda(Ti),M} = R_{\lambda(Ti)} c_{Ti,M} q_M + b_{\lambda(Ti)} \quad (3)$$

Carbon calibration was set up using reference materials of steels and cast iron, calibration of hydrogen was based on the TiH_2 layer on Ti [23, 24] and pure titanium. Calibration function of nitrogen, Figs 1c, 1d was established based on reference samples of steels, with the highest nitrogen concentration of 0.896 wt. %, in the sample NSC4-C (MBH Analytical Ltd., UK), see Fig 1c. The point corresponding to TiN does *not* fit to this calibration function and was excluded from its calculation. The same applies to the points corresponding to Coronite and the Ti_3.1E17N sample. This discrepancy is discussed below. Sputter rate q_{TiN} of the TiN sample was calculated [15] using the Ti calibration, established with the other Ti-containing samples with known sputter rates and pure Fe as a blank sample, see Fig. 1a. In the calibration measurements, the intensities were recorded after letting the discharge run for a while to stabilize (30 seconds).

[2] In the plots in Fig 1, sputter rates (originally as sputtered mass per second) are treated as 'sputter factors', i.e., as dimensionless quantities relative to the sputter rate of pure iron at the same glow discharge conditions, q_M/q_{Fe}.

View Article Online
DOI: 10.1039/D6JA00037A

In depth profile analyses of the N-implanted samples, signal intensities were collected as functions of the time of sputtering, *t*, and raw data (intensities-versus-time) were converted into quantitative depth profiles (concentrations-versus-depth) by a common GDOES quantification procedure [15]: First, for every point *t* of the depth profile, the $c_{E,M}(t)q_M(t)$ products were calculated for Ti, N, Nb, H, C, based on the recorded intensities $I_{\lambda(E),M}(t)$ and the respective calibrations, Eqn (2) or Eqn (3). Instantaneous sputter rate $q_M(t)$ was then calculated using the fact that, in every point of the depth profile, the sum of the concentrations of the mentioned elements is equal to 100%:

$$\sum_E c_{E,M}(t)q_M(t) = q_M(t)\sum_E c_{E,M}(t) = q_M(t).(100\%) = q_M(t) \quad (4)$$

With $q_M(t)$ already known, sample composition as function of time was established from the $c_{E,M}(t)q_M(t)$ products. The conversion of the time scale into depth proceeds as follows: Provided that the concentrations and sputter rates are in mass units, the mass of the sample sputtered off within the time interval dt is

$$dm = \rho_M.\pi r^2.dh = q_M(t)dt \quad (5)$$

where ρ_M is the density of the sample material and *r* is the anode radius, i.e., the radius of the analyzed spot. The depth $h(t)$ as function of the time of sputtering was then established by integrating Equation (5):

$$h(t) = \frac{1}{\pi r^2}\int_0^t \frac{q_M(\tau)}{\rho_M(\tau)}d\tau \quad (6)$$

The density of the matrix $\rho_M(\tau)$ may vary, as the composition of the sample varies with depth. For the calculation of $h(t)$ using Eqn (6), sample density was treated as follows: in the Ti-N system, the density of pure Ti is ρ_{Ti} = 4.51 g cm^3 and the density of TiN is ρ_{TiN} = 5.40 g cm^{-3}. The density of a matrix consisting of titanium with nitrogen at a concentration c_N [at. %] was then taken as the weighted average of ρ_{Ti}, ρ_{TiN} :

$$\rho_M(t) = \left[2c_N(t)\rho_{TiN} + \left(100 - 2c_N(t)\right)\rho_{Ti}\right]/100 \quad (7)$$

Concerning the TiNb alloys, the densities of Ti25Nb and Ti55Nb are 5.09 and 6.10 g cm^{-3}, respectively. The density of the TiNb matrix with nitrogen was treated analogically as in the Ti-N case, except that, instead of ρ_{Ti}, the appropriate ρ_{TiNb} density was used, and for the corresponding (Ti,Nb)N nitride, a value by 20% higher was taken, in analogy with titanium without Nb, as ρ_{TiN}/ρ_{Ti} = 1.20. Absolute sputter rate of pure Ti at the given discharge conditions was 38 nm s^{-1}. It was established as described in Ref. [15], based on the Fe-3313 thickness standard (Kocour, Chicago, IL, USA) and confirmed by depth measurements of the erosion crater after a given time of sputtering, by a scanning profilometer (DEKTAK XT, Bruker Corp.). Total amount of nitrogen in the N-implanted samples, [N atoms cm^{-2}], was calculated by the integration of the respective nitrogen depth profiles[3]. When doing that, the first several points of the depth profile (up to ≈1 s), with higher intensities of C, H, N, were not included, as they reflect largely the desorption of atmospheric gases from the walls of the

[3] Total amount of an element *E*, if it is present solely in a surface layer, can also be established by integrating the quantity $I_E(t)/R_E$ over the time interval from zero to such a time at which the signal $I_E(t)$ vanishes, i.e., without even knowing sample density as function of depth or the sputtering time, $\rho_M(h)$, $\rho_M(t)$ [15].

View Article Online
DOI: 10.1039/D6JA00037A

spectral source and the sample surface upon the discharge startup, rather than the implanted nitrogen.

Actual amount of implanted nitrogen in the Ti_3.1E17N sample was confirmed by the Rutherford Backscattering Spectrometry (RBS). The RBS spectra were acquired using a 3.75 MeV helium ion beam. The backscattered helium ions were detected using an Ultra-Ortec PIPS detector positioned at a laboratory scattering angle of 170° in the Cornell geometry. The ion current during RBS measurements was approximately 5 nA. To mitigate sample degradation by the analysis ion beam, multiple RBS spectra were collected at different beam spots. The final spectrum represents the sum of these individual spectra. Elemental concentrations were determined using the SIMNRA software [25] applying the relevant non-Rutherford cross-sections.

The mentioned sample was also analysed by another complementary method, SIMS, to confirm the conformance with the corresponding GDOES depth profile. The SIMS analysis was made using the IMS 7f SIMS instrument (Cameca SAS, France). It was operated in positive primary ion (10 keV impact energy, 100 nA ion current, O_2^+ species, scanned area 150 µm)/ positive secondary ion ($^{14}N^+$, $^{48}Ti^+$) mode at mass resolution 1200. The depth scale was calibrated using a stylus profilometer DEKTAK XT (Bruker Corp.) and the assumption of constant sputter rate[4]. The concentration scale was calibrated using the indirect method mentioned below.

Results

It was found that, not only the nitrogen intensity response for TiN is incompatible with the calibration curve based on nitrogen-alloyed steels, but, as described above, nitrogen calibration based on steels is not good for the N-implanted samples, either: the thereby obtained total nitrogen content does not correspond to the declared nitrogen fluences. The problem obviously lies in the nitrogen calibration, namely in the emission yield of the nitrogen line used, R_N. To cope with this situation, in the first step, the data interpretation procedure was reversed, i.e., a selected N-implanted sample, Ti_3E17N (pure titanium implanted with nitrogen at 3.0×10^{17} at. cm^{-2}), was taken as a reference, and the emission yield R_N was set so that the integrated quantified nitrogen depth profile yields the 'correct' total amount of nitrogen, equal to the declared fluence in that 'reference' sample. This approach can be called an 'indirect calibration'. The resulting depth profile of the sample Ti_3E17N, quantified with this emission yield R_N, is in Fig. 2. Its correctness was verified by the RBS method on a very similar sample, N-implanted titanium at the fluence of 3.1×10^{17} at. cm^{-2}, see above in the section "Experimental". Further analyses showed that this 'indirect calibration' works reasonably well for the samples implanted by low fluences, and, also, the shape of nitrogen depth profiles in such samples was found to be close to gaussian depth distributions, typical for ion implantation [19, 26]. However, at higher fluences, saturation of the nitrogen concentration in the implanted

[4] Not only the sputter rates in SIMS and GDOES differ by the magnitude, but they are in fact different quantities: in GDOES it is the *net* sputter rate, affected by redeposition and self-sputtering [15], while in SIMS and other high vacuum methods using ion beams those phenomena do not occur.

View Article Online
DOI: 10.1039/D6JA00037A

Fig. 1

Calibration curves of Ti, Nb and N. At the plots, abscissa denotes the respective signal intensity. On the ordinate, each magenta point denotes the concentration of the element, *c*, in the respective sample. Red points denote the respective (*c.q*) product, while the red and the magenta points belonging to the same sample are connected by a vertical turquoise line. Calibration curve is defined by the red points. Calibration function of N depicted here is defined by the steel samples. The sputter rate (sputter factor) of TiN, q_{TiN}, was calculated based on the Ti calibration, (a), so that the respective (*c.q*) point, blue, lies on the Ti calibration curve established by the other Ti-containing samples.

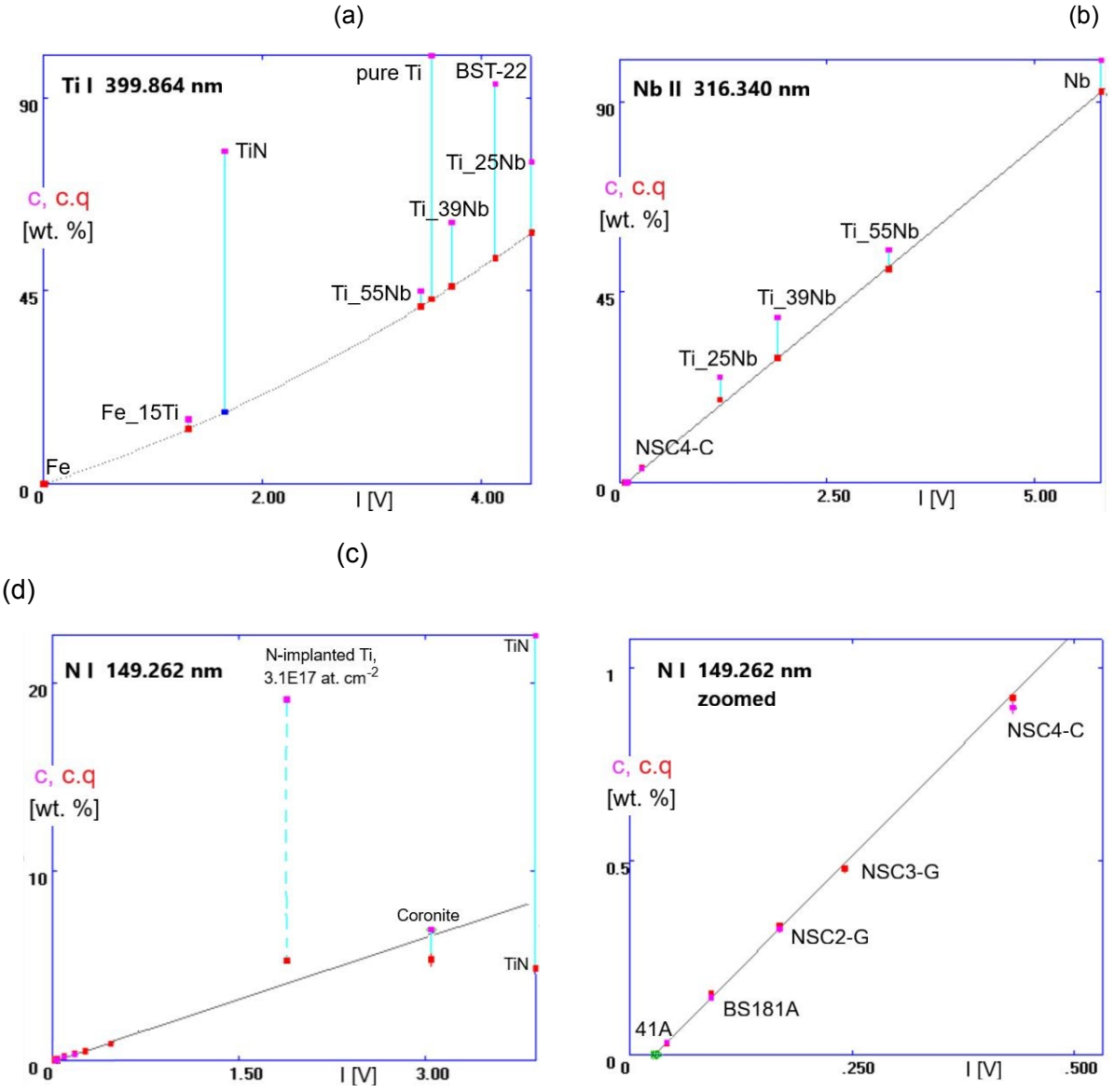

layer takes place, i.e., depth profile of nitrogen gets flattened in the vicinity of the maximum, see Fig 3, and the total nitrogen amount in the implanted layer does not further rise with an increasing fluence. Much more realistic results for samples implanted with high nitrogen fluences were obtained by using the emission yield R_N derived from the intensity response of the TiN sample, as depicted in the nitrogen calibration in Fig. 1c. This can be demonstrated by the plots in Figs 3, 4. The three values of the emission yield of nitrogen mentioned above,

i.e., $R_N(steels)$, $R_N(Ti\_3E17N)$ and $R_N(TiN)$ are 432, 233 and 703 mV/wt.%, respectively[5]. They differ quite significantly, which violates the basic GDOES paradigm, i.e., that emission yields are virtually independent of the matrix under study[6].

Fig. 2

Depth profile of sample Ti_3E17N. The quantification was performed with R_N=233 mV/wt.%, according to the declared fluence of 3.0x10^{17} at.cm^{-2} (an 'indirect calibration'). Ordinate: atomic concentrations of Ti, N, Nb, C, H. Multiplicative scaling factors specified in the caption were applied, to match the concentration range displayed. They are indicated in the legend, after asterisk (*) at the symbol of each element. The black dashed line represents the calculated sputter rate, q_I, in nm s^{-1}. Realistic data reflecting the implantation profile start after the local minimum of N at ≈10 nm. The beginning of the depth profile reflects gas desorption at the discharge startup and/or prospective contamination of the sample surface.

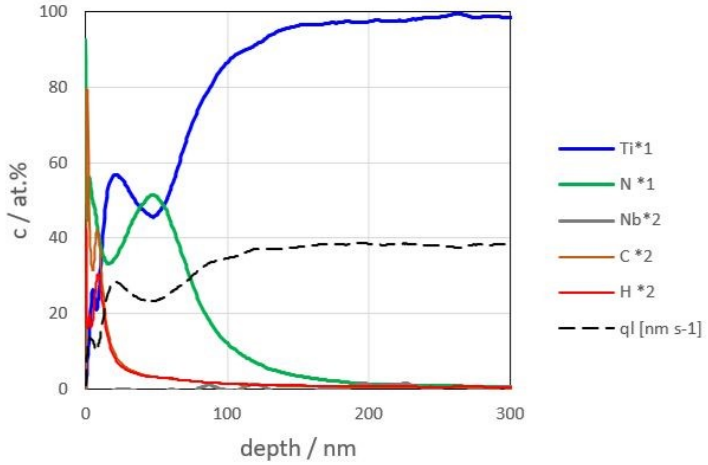

[5]Absolute values of $R_{\lambda(E)}$ do not have a fundamental significance, as they depend on the sensitivity setting of the respective analytical channel (light detector), which is instrument dependent. However, the ratios of emission yields of the same channel in the analysis of different matrices, as discussed here, bear some information about the physics taking place.

[6] This paradigm applies with a good accuracy to commonly used 'analytical' lines of non-gaseous elements. However, this is not a universal rule and deviations from this calibration model exist, especially in the analysis of gaseous elements, e.g. oxygen [43].

View Article Online
DOI: 10.1039/D6JA00037A

Fig. 3

Depth profiles of samples Ti25Nb_3E17N (a) and Ti25Nb_6E17N (b), as quantified using R_N=233 mV/wt.% (an 'indirect calibration' based on the sample Ti_3E17N). The resulting nitrogen concentration in the latter sample (Ti25Nb_6E17N) is unrealistically high and that profile is not correct. Note that in the plots are concentrations in atomic percent, while the designation Ti25Nb means 25% weight percent of niobium.

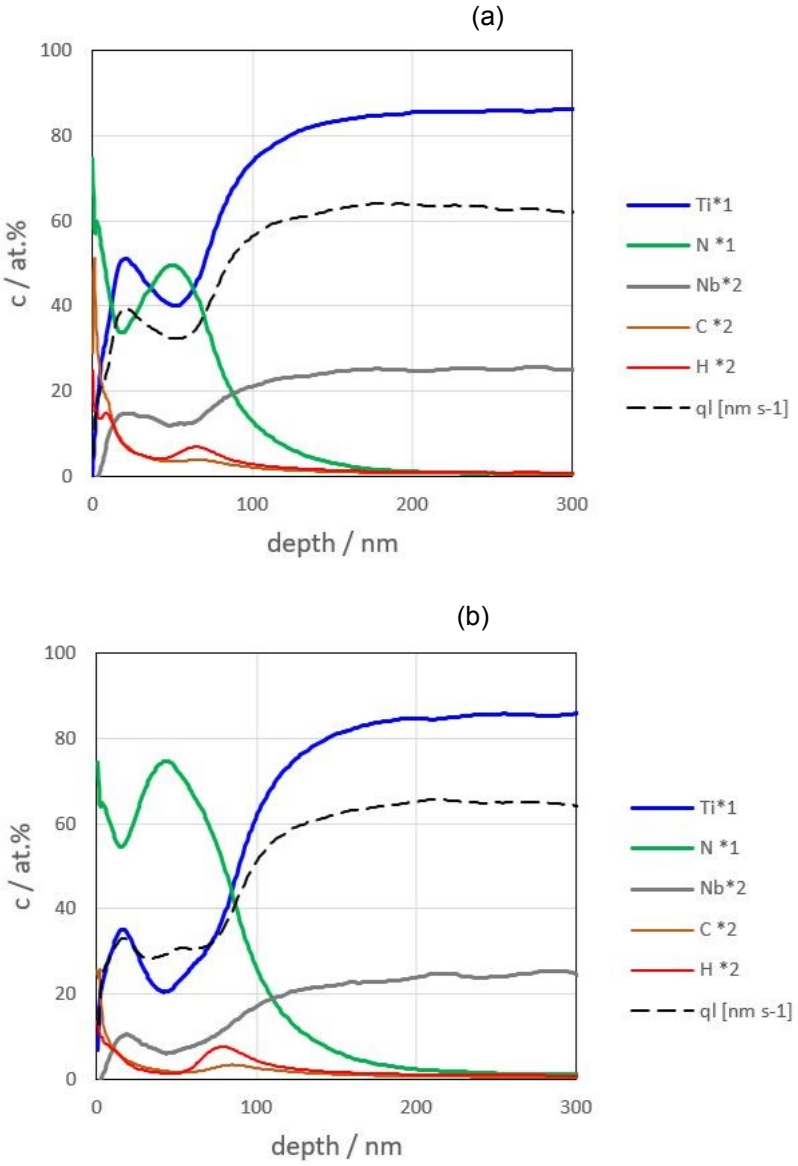

View Article Online
DOI: 10.1039/D6JA00037A

Fig. 4

(a): depth profile of sample Ti25Nb_12E17N, quantified with R_N=233 mV/wt.%, (unrealistic, incorrect).
(b): depth profile of the same sample, quantification derived from the intensity response of the stoichiometric TiN, with R_N=703 mV/wt.%.

(a)

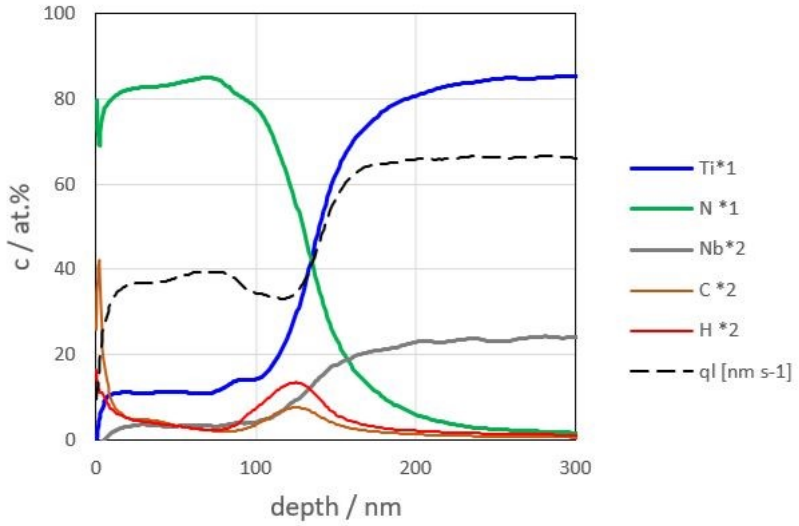

(b)

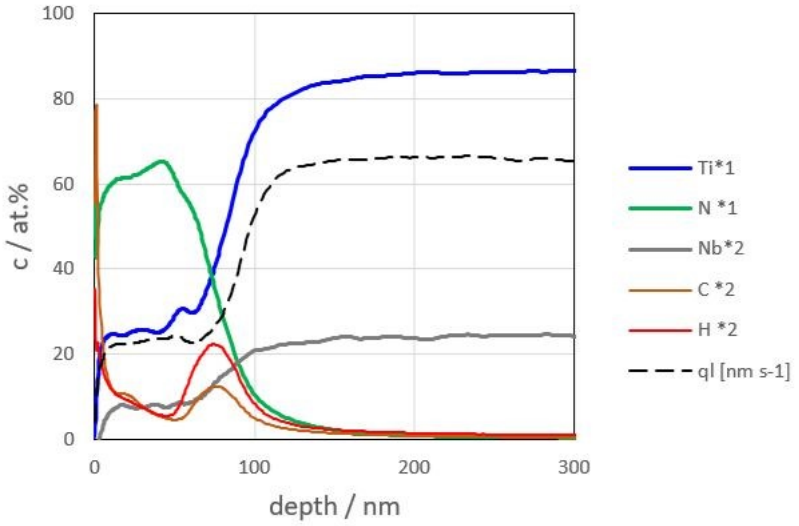

View Article Online
DOI: 10.1039/D6JA00037A

Fig. 5

Depth profile of sample Ti55Nb_24E17N, quantification derived from the intensity response of the stoichiometric TiN, with R_N=703 mV/wt.%. Similar as before, Ti55Nb means 55 wt.% of niobium.

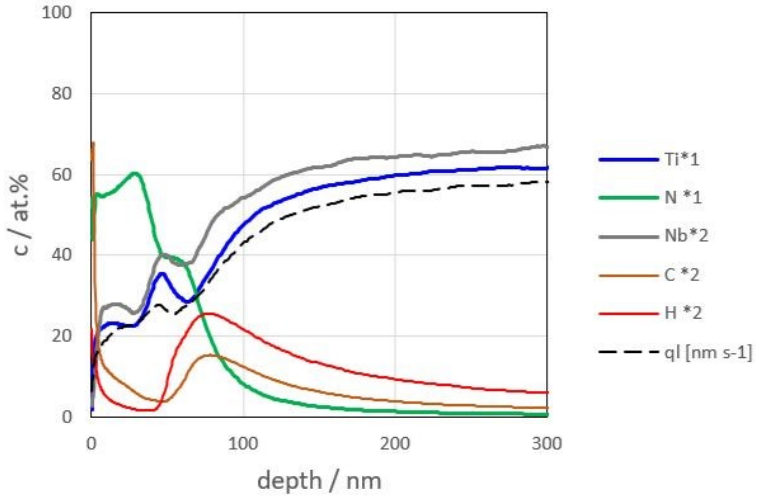

To complete the results concerning the present series of samples, there are three more features worth to mention:

1. At extremely high nitrogen fluences, a distinct separate layer is formed at the interface between the implanted layer on the top and the base metal, with a markedly lower nitrogen concentration, and a stoichiometry approaching $(Ti, Nb)_2N$. See Fig 5.
2. At the Ti-Nb samples, the region just beneath the implanted layer is enriched with hydrogen and carbon: see the depth profiles in Figs 3, 4, 5. Hydrogen is known to affect GDOES intensities of some other elements to some extent [24, 27]. In the present analyses, no 'hydrogen corrections' of the Ti, N and Nb signals were made. The TiH_2 sample used for hydrogen calibration was not certified and the resulting concentrations of H, as shown in Figs 3, 4, 5, might be slightly overestimated.
3. At the Ti-Nb samples, niobium behaves similarly as titanium, i.e., the Nb/Ti ratio remains virtually constant throughout the whole depth profile. Only in the $(Ti,Nb)_2N$ layer at the interface, formed with the highest nitrogen fluences and mentioned above under point 1, the Nb/Ti ratio is slightly higher than in the base metal, by about ≈10%.

As mentioned, total amount of nitrogen in the N-rich layer of the samples was established by the integration of the respective depth profiles, quantified as described above, with R_N depending on the nitrogen fluence: R_N=233 mV/wt.% for the 'lower' N fluences, ≤ 3.0×10^{17} at. cm^{-2}, and R_N=703 mV/wt.% for the 'higher' fluences, > 6.0×10^{17} at. cm^{-2}. The results are in Table 1 and are also plotted in Fig. 6. The fluence of 6.0×10^{17} at. cm^{-2} lies in the 'intermediate' region between the 'low' and the 'high' fluences and quantification with none of the two mentioned R_N values yields an acceptable total amount of nitrogen. Hence, the values in the parentheses in Table 1 were calculated as the average of the two figures resulting from the quantification with either R_N mentioned. It should be noted that the three valid digits in the numbers in Table 1 do *not* imply anything about the level of accuracy of those results: estimated relative uncertainty of the reference value indicated by the asterisk, for sample Ti_3E17N, is several percent, and, consequently, so would also be a possible

systematic bias of the results for the other 'lower-fluence' samples, because they are linked to that reference value via the emission yield R_N.

Table 1

Total amount of nitrogen in the N-implanted samples of Ti and the Ti25Nb and Ti55Nb alloys as resulting from integrated GDOES depth profiles, quantified using the proper value of R_N (see the text).

N fluence [10^{17} at. cm^{-2}]	Ti [10^{17} at. cm^{-2}]	Ti25Nb [10^{17} at. cm^{-2}]	Ti55Nb [10^{17} at. cm^{-2}]
1.0	0.87	0.81	1.21
3.0	3.00*	3.11	3.36
6.0	(5.1)	(4.8)	
9.0	4.65	5.41	5.26
12	5.97	6.37	5.07
18	4.80		
24		5.06	4.60

* Reference value for low fluences up to 3.0x10^{17} at. cm^{-2} N.

Fig. 6

Total amount of nitrogen in the N-implanted samples as function of the nitrogen fluence, resulting from the GDOES depth profiles. The dashed line represents the identity function, $y = x$.

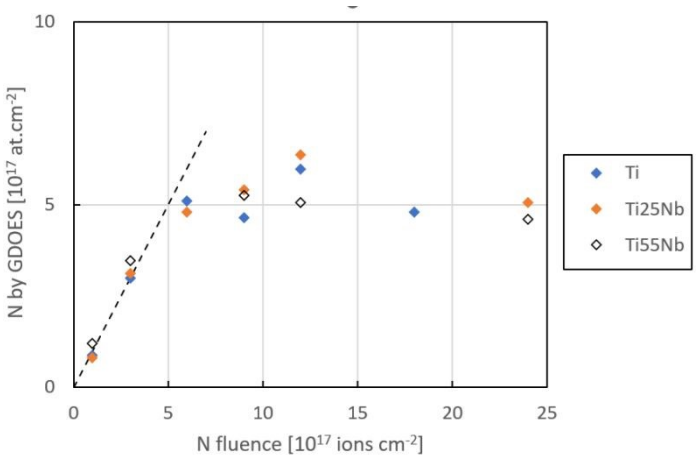

Discussion

Eqn (2) means that, except for a low spectral background, $b_{\lambda(E)}$, emission intensities of the lines of an element are proportional to the product $c_{E,M}q_M$. The rationale behind this is that the intensity $I_{\lambda(E),M}$ is proportional to the number density n_E^{vol} of the atoms of element E in the volume of glow discharge plasma, which is controlled by dynamic equilibrium between the source flux of the atoms of element E entering the plasma due to sputtering, $\Phi_{E(in)}$,

$$\Phi_{\mathrm{E}}(in) \propto c_E q_M \qquad (8)$$

View Article Online
DOI: 10.1039/D6JA00037A

and the sink flux, $\Phi_{E(out)}$, of atoms of element E leaving the plasma, being redeposited on the anode wall (see Fig. 7). This flux is proportional to the impingement flux of element *E*, which itself is proportional to the number density n_E^{adj} next to the anode wall [36] and a proportionality constant ξ_E called the *sticking coefficient* [28] of element *E*:

$$\Phi_{\mathrm{E}}(out) = \frac{1}{4}\xi_E \overline{v}_E n_E^{adj} \qquad (9)$$

where $\overline{v}_E$ is the average velocity of the atoms of element *E* in the plasma and the superscript 'adj' means that Eqn (9) concerns the region (a thin layer) adjacent to the anode wall. Sticking coefficient expresses the probability that an atom of element *E* hitting the wall gets trapped. The transport of the analyte within the discharge cell is described by the equation of diffusion, with boundary conditions defined by the source- and sink fluxes, $\Phi_{E(in)}$, $\Phi_{E(out)}$. Its solution is the number density distribution of the analyte, $n_{E(r, z)}$, in the discharge cell. For the Grimm-type cell geometry, diffusion equation was solved both analytically [37] and numerically by computer modelling [34], see Fig. 7. The task here is to assess how the analyte number density in the plasma (and consequently the emission intensity I_E) depends on the fundamental parameters mentioned, in particular, the sticking coefficient ξ_E.

At the steady state, the source- and sink fluxes of the analyte atoms, integrated over the respective surfaces of the cell, are equal:

$$\Phi_{\mathrm{E}}(in) = \Phi_{\mathrm{E}}(out) = \Phi_{\mathrm{E}} \quad , \qquad (10)$$

and the analyte transport within the cell can be approximately described in analogy with the equivalent electrical circuit depicted in Fig. 8.

Fig. 7

The geometry of the Grimm-type GDOES discharge cell. The level lines illustrate a typical number density distribution in the plasma, n_E [atoms cm^{-3}], of an element (Cu) sputtered from the sample. Adopted with permission from Ref [34], Copyright (1998) Elsevier.

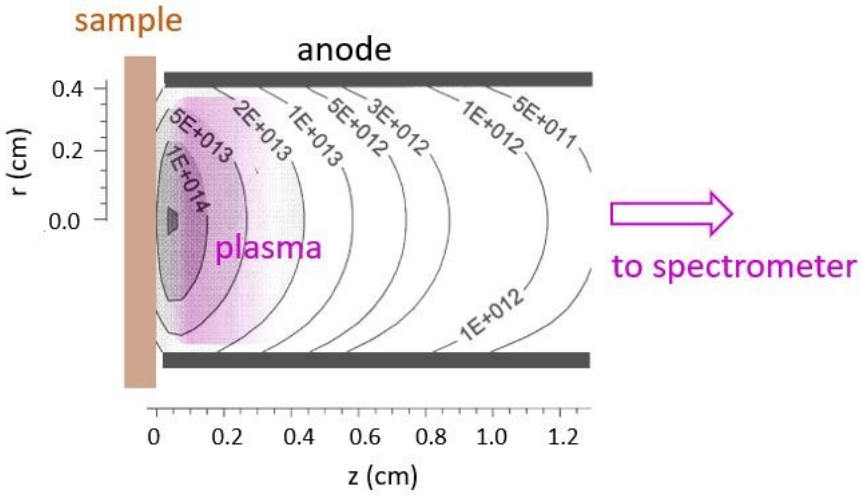

View Article Online
DOI: 10.1039/D6JA00037A

Fig. 8

Analyte transport and redeposition in the discharge cell: an equivalent circuit. In this analogy, the current *i* corresponds to the flux of element *E* in the plasma, Φ_E, the voltages U_v, U_a correspond to the number densities n_E^{vol} and n_E^{adj}, respectively, resistor R_D corresponds to l/D_E, see Eqn (12) and resistor R_ξ, corresponds to $4/(\xi_E \bar{v}_E)$, see Eqn (9).

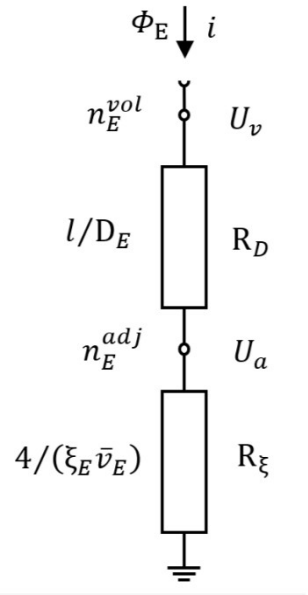

In the discharge cell, the transport of the sputtered material proceeds by diffusion and the number density n_E in the plasma follows the first Fick's law:

$$\Phi_E(z,r) = -D_E \nabla n_E(z,r) \qquad (11)$$

where D_E is the diffusion coefficient of element *E* in the plasma and ∇n_E is the gradient of n_E. Integrating this over all possible diffusion paths and the plasma volume, we can write

$$\Phi_E = c_E q_M = \frac{D_E}{l}\left(n_E^{vol} - n_E^{adj}\right) \qquad (12)$$

where n_E^{vol} is the number density of element *E* in the volume of the plasma and *l* is a characteristic diffusion length, related to the anode radius. Unlike in preceding sections, $c_E q_M$ is considered here in atomic units instead of mass, so that the flux Φ_E is equal to $c_E q_M$. The quantities *l*, n_E^{vol} may seem to be defined somewhat vaguely, but important is that Eqn (12) holds also on the microscopic level, for every point in the plasma and every bit of a diffusion line, hence, the integration is justified, and n_E^{vol} represents some kind of averaged number density of element *E* in the glowing region.

Combining Eqns (9) – (12), we get

$$n_E^{vol} = c_E q_M \left(\frac{l}{D_E} + \frac{4}{\xi_E \bar{v}_E}\right) \quad , \qquad (13)$$

Consequently, emission yield $R_{\lambda(E)}$ depends on the diffusivity and the sticking coefficient of element *E* as follows:

$$R_{\lambda(E)} \propto \frac{l}{D_E} + \frac{4}{\xi_E \bar{v}_E} \quad . \qquad (14)$$

Substituting realistic parameters of the process, i.e., T = 800 K [39], $p(Ar)$ = 5.3 hPa and l = 1 mm for a 2.5 mm-diameter anode, the proportionality relation, Eqn (14), for atomic nitrogen becomes

$$R_{\lambda(N)} \propto 2.6 + \frac{0.36}{\xi_N} \quad , \qquad (15)$$

and, if a substantial degree of nitrogen recombination occurs in the plasma, for molecular nitrogen, N_2, it will be

$$R_{\lambda(N)} \propto 4.8 + \frac{0.52}{\xi_N} \quad , \qquad (16)$$

while the first term on the right side represents diffusion in the volume and the second term refers to redeposition (entrapment rate) on the walls. This means that, both for atomic and molecular nitrogen, relative contributions to the emission yield $R_{\lambda(N)}$ of the diffusion in the cell and the wall entrapment rate are comparable, although, for $\xi_N \rightarrow 1$, the former would be greater. For $\xi_N < 1$, relative importance of the entrapment rate rises, and emission yield goes up also. Background data for Eqns (14) to (16) are in Table 1. The table contains also titanium. In most papers dealing with computer modelling of discharges, it is assumed that, for metals and other non-gaseous species, the entrapment rate on the walls virtually does not depend on the composition of the redeposited material and $\xi_E \rightarrow 1$, because the temperature of the anode is relatively low. Emission yields are then controlled solely by diffusion, in accordance with Ref. [42].

Table 2

Underlying data for Eqns (14) to (16). Diffusion coefficients (column 4) were calculated based on the diffusivity of molecular nitrogen in argon at T= 293 K and the atmospheric pressure, D=0.19 cm^2 s^{-1} [41], and the following proportionality relations: $D \propto T^{1.75}/p$, $D \propto 1/\sigma$, $D \propto 1/\sqrt{M_{X=Ar}}$ [36], where σ is the respective collision cross section with argon and $M_{X\text{-}Ar}$ is the reduced atomic (molecular) mass of the couple X-Ar, X being the species under study. The collision cross sections come from literature[7], see column 4. The figures refer to the experimental parameters mentioned in the text (T = 800 K, p = 5.3 hPa, l = 1 mm).

	M_r	$M_{X\text{-}Ar}$	$\sigma_{X \text{ in } Ar}$ [10^{-20} m^2]	$D_{X \text{ in } Ar}$ [cm^2 s^{-1}]	$\bar{v}_X$ [m s^{-1}]	$l/D_{X \text{ in } Ar}$ [10^{-4} cm^{-1} s]	$4/\bar{v}_X$ [10^{-4} cm^{-1} s]
N	14	10.4	221 [40]	383	1096	2.6	0.36
N_2	28	16.5	320 [40]	210	775	4.8	0.52
Ti	47.9	21.8	200 [38]	292	592	3.4	0.68

As suggested by relations Eqn (14) to Eqn (16), the likely explanation of the observed nitrogen signal response in different matrices, i.e., $R_N(Ti\_3E17N) < R_N(steels) < R_N(TiN)$, consists in *different sticking coefficients of nitrogen on the different materials redeposited on the anode*. In particular, for samples implanted by lower fluences of N, the Ti/N ratio of the

[7] Experimental collisional cross sections of N in Ar and N_2 in Ar greatly differ from the values calculated using the commonly reported collisional diameters.

View Article Online
DOI: 10.1039/D6JA00037A

redeposited material is higher than with samples implanted by high fluences of N, and the TiN sample. Moreover, redeposition occurs not only on the anode, but thermalized atoms hit the sample surface as well, and, if the sample surface consists at least partly of elemental Ti, nitrogen from the plasma can also be (temporarily) trapped there and eventually re-sputtered. Here comes into play also the Ti enhancement of a TiN surface by preferential sputtering[8] [28]. It is well known that nitrogen has a high affinity to titanium and undergoes chemisorption on a Ti surface, through Ti-N bonds, increasing thereby the sticking coefficient. This is what causes the well-known 'gettering' effect and is widely used in vacuum technology, e.g., in ion-sorption pumps. On the contrary, if the surfaces surrounding the plasma are covered largely by TiN instead of Ti, the sticking coefficient of nitrogen, ξ_N, dramatically drops. This was clearly demonstrated, e.g., in reactive magnetron sputtering [29- 31]. There is also a Ti-N phase with a higher N/Ti ratio, TiN_2, [32], however, its formation was not confirmed here. Because emission yields in GDOES rise as the respective sticking coefficients drop, as follows from Eqn (14) , the empirically established relation $R_N(Ti\_3E17N) < R_N(TiN)$ can be explained by $\xi_N(Ti) > \xi_N(TiN)$. The magnitude of the differences in R_N between Ti and TiN reported above under Results implies that the sticking coefficient $\xi_N(TiN)$ on the anode should indeed be several times lower than $\xi_N(Ti)$. It may well be, that the sticking coefficient of nitrogen in the analysis of N-alloyed steels, $\xi_N(steel)$, is somewhere in between $\xi_N(Ti)$ and $\xi_N(TiN)$, which would plausibly explain the observed relation between emission yields of the mentioned nitrogen line in the analysis of those three matrices. Also, the fact that total amounts of nitrogen, as resulting from the analysis, exceed the declared fluence in the Ti25Nb_3E17N, Ti55Nb_3E17N samples when the Ti_3E17N sample is taken as a reference (see Table 1), suggest that sticking coefficient for nitrogen in the TiNb alloys also depends on the titanium concentration, so that $\xi_N(Ti55Nb) < \xi_N(Ti25Nb) < \xi_N(Ti)$. Obviously, using the sample Ti_3E17N as a reference is rather a virtue of necessity than a universal solution. However, for these 'low fluence' samples, the thereby obtained results are still much better than with TiN as a reference, in which case the discrepancy would not be 4% (Ti25Nb_3E17N) or 12% (Ti55Nb_3E17N) but the nitrogen results $(c_N q)$ would be biased by a factor of ≈2-3.

For completeness, there is one more aspect worth to mention: whilst the response of TiN was measured after a 30s long 'preburn' period, the whole depth profile of a N-implanted sample lasts only few seconds (e.g., in sample Ti_3E17N, the first 1.4 s after the startup was not considered (outgassing of the anode), and, after another 1.3 s, the peak of the implanted profile was reached). Hence, temporal characteristics may also play a role. It appears that, except of sample heating and the changes in the sticking coefficient ξ_N, all the other transient processes in the plasma are too fast to affect the signal-time relations mentioned here [33].

Conclusions

GDOES is a fast and affordable multi-element depth profiling method, suitable for the analysis of nitrogen in coatings and N-implanted materials. Central role in the analytical interpretation of line intensities in GDOES have the *emission yields*, R_E, expressing relative

[8] Nitrogen has a slightly higher sputtering yield than titanium when TiN_x is sputtered. Therefore, a surface layer develops, few monolayers thick, with a higher Ti concentration than in the material underneath, so that the Ti/N ratio in the resulting flux of sputtered atoms is the same as below this modified surface layer.

View Article Online
DOI: 10.1039/D6JA00037A

sensitivity for the given element of the emission line used. In the conventional approach, emission yields are considered as independent of the matrix analysed. This applies to the analysis of metals and other non-gaseous elements with high sticking coefficients on the surfaces surrounding the plasma, $\xi_E \rightarrow 1$. In the present work, it was found that this assumption does not hold for nitrogen analysis in N-implanted titanium and Ti-Nb alloys. Due to a much higher sticking coefficient of nitrogen on the Ti or Ti-Nb surface than on the surface of TiN_x or $(Ti,Nb)N_x$, emission yield of the N I 149.262 nm line varies with the concentration of nitrogen in the matrix. This feature is not common in the analysis of other materials and quantification schemes implemented in commercial GDOES spectrometers must be used with caution in applications like this.

For Ti, Ti-Nb samples implanted with nitrogen at lower fluences, up to ≈ $3x10^{17}$ at. cm^{-2}, an implanted sample with a known fluence can be taken as a reference and the quantification of such depth profiles can be performed using the emission yield R_N established accordingly, so that the integrated depth profile of nitrogen yields the total amount of nitrogen, equal to the implanted fluence. At such fluences, the shape of nitrogen depth profiles is close to the gaussian distribution of nitrogen with depth, typical for ion implantation profiles [19], with the maximum at several tens of nanometers below the surface. For very high nitrogen fluences, greater than ≈ $6x10^{17}$ at. cm^{-2}, quantification of the depth profiles can be done with R_N derived from the intensity response of stoichiometric titanium nitride. At such fluences, saturation of the nitrogen concentration in the implanted layer takes place, at a level close to- or slightly above 50 at. %, i.e., the depth profile of nitrogen gets flattened in the vicinity of the maximum. Furthermore, total amount of nitrogen in the implanted layer does not further rise with an increasing fluence. At the highest fluences approaching 12-24 $x10^{17}$ at.cm^{-2}, a distinct separate layer is formed at the interface between the surface-near zone and the base metal, with a lower nitrogen concentration and a stoichiometry approaching $(Ti,Nb)_2N$. A similar behaviour was described four decades ago, with nitrogen implantation at very high fluences into pure titanium, resulting in the formation of the Ti_2N phase [35].

It was shown how the observed signal response of nitrogen depends on the number density n_N^{vol} of nitrogen atoms in the plasma. Not only n_N^{vol} is controlled by the flux of nitrogen atoms sputtered from the cathode and entering the plasma, proportional to ($c_N.q$), but also by the transport of nitrogen in the plasma and its redeposition on the walls. These processes depend on the diffusivity of nitrogen in the plasma and the sticking coefficient of nitrogen on the walls and are described by relations Eqn (13) and Eqn (14). The discussion of this topic presented here refines a somewhat simplistic treatment of n_N^{vol} in Ref. [22]. Analogous mechanism might be at play in the analysis of other gaseous elements also.

.

View Article Online
DOI: 10.1039/D6JA00037A

Acknowledgments

Ion implantation experiments were performed with the support of the Grant Agency of the Czech Technical University in Prague (grant No. SGS24/121/OHK2/3T/12) and VVI CENAKVA Research Infrastructure (ID 90238, MEYS CR, 2023-2026).

RBS analysis was carried out at the CANAM (Centre of Accelerators and Nuclear Analytical Methods) infrastructure LM 2015056.

SIMS and stylus profilometry results were obtained using the CICRR infrastructure, which is financially supported by the Czech Ministry of Education, Youth and Sports - project LM2023041.

GDOES analyses were funded by the Ferroic Multifunctionalities project, supported by the Ministry of Education, Youth, and Sports of the Czech Republic. Project No. CZ.02.01.01/00/22_008/0004591, co-funded by the European Union.

Author Contributions:

Z. Weiss: Conceptualization, GDOES analyses, interpretation of GDOES data; V. Smola, M. Lebeda, P. Vlčák: sample preparation and ion implantation experiments; J. Lorinčík: SIMS analyses; I. Elantyev: stylus profilometer measurements; P. Malinský: RBS analyses

References

1. J. Musil, Hard and superhard nanocomposite coatings, *Surf. Coat. Technol.* 125 (2000) 322–330, https://doi.org/10.1016/S0257-8972(99)00586-1
2. H. Holleck, Material selection for hard coatings*, J. Vac. Sci. Technol. A* 4, 2661–2669 (1986), https://doi.org/10.1116/1.573700
3. J.-E. Sundgren, A. Rockett and J.E. Greene, Microstructural and microchemical characterization of hard coatings, *J. Vac. Sci. Technol. A* 4 (1986) 2770-2783, https://doi.org/10.1116/1.573678
4. W. Lengauer, J. Bauer, A. Guillou, D. Ansel, J.-P. Bars, M. Bohn, E. Etchessahar, J. Debuigne, P. Ettmayer, WDS-EPMA Nitrogen Profile Determination in TiN/Ti Diffusion Couples Using Homotypic Standard Materials, *Mikrochim. Acta* (1992) 107, 303-310, https://doi.org/10.1007/BF01244485
5. J. Xu, C.D. Lane, J. Ou, S.L. Cockcroft, D.M. Maijer, A. Akhtar, Y. Marciano, Diffusion of nitrogen in solid titanium at elevated temperature and the influence on the microstructure, *J. Mater. Res. Technol*. 12 (2021) 125-137, https://doi.org/10.1016/j.jmrt.2021.02.073
6. S. Hofmann, Characterization of nitride coatings by Auger electron spectroscopy and X-ray photoelectron spectroscopy, *J. Vac. Sci. Technol*. A 4 (1986) 2789-2796, https://doi.org/10.1116/1.573680
7. H.A. Jehn, E. Grallath, Y. LeRoux Strydom, S. Hoffmann, Comparison of AES Analyses of transition-metal Nitride Coatings with Carrier-gas Heat Extraction Analyses, *Surf. Interface Anal.* 16 (1990), 540-545, https://doi.org/10`.1002/sia.7401601112

8. S. Baunack, V. Hoffmann, W. Zahn, Quantitative nitrogen analysis by Auger electron spectrometry and glow discharge optical emission spectrometry, *Microchim. Acta* 156 (2007) 69–72 , https://doi.org/10.1007/s00604-006-0587-9
9. W. Pamler, M. Hüttinger, W. Bensch, Sputtering effects in Auger depth profiles of TiN thin films, *Thin Solid Films* 174 (1989) 143-148, https://doi.org/10.1016/0040-6090(89)90882-1
10. V. Smola, P. Vlcak, T. Horazdovsky, J. Sepitka, J. Drahokoupil, Z. Tolde, M. Lebeda, A. Skolakova, K. Masek, Effect of argon ion sputter etching on the surface chemistry and surface properties of binary Ti-Nb alloys and commercially pure titanium, *Surf. Interfaces* 80 (2026) 108317. https://doi.org/10.1016/j.surfin.2025.108317
11. D. Pietersen, W.J. Strydom, The determination of nitrogen in titanium nitride coatings using the nuclear reaction ^{15}N (p, αγ) ^{12}C, *Nucl. Instrum. Methods Phys. Res. B* 35 (1988) 467-471, https://doi.org/10.1016/0168-583X(88)90313-8
12. V. Havránek, V. Hnatowicz, J. Kvítek, J. Musil, V. Poulek, Determination of nitrogen content in thick layers by proton backscattering, *Nucl. Instrum. Methods Phys. Res. B* 47 (1990) 433-438, https://doi.org/10.1016/0168-583X(90)90623-3
13. F. Abautret and P. Eveno, Diffusion of nitrogen implanted in titanium nitride (TiN_{1-x}), *Revue Phys. Appl.* 25 (1990) 1113-1119, https://doi.org/10.1051/rphysap:0199000250110111300
14. R. Payling, T. Nelis, et al., *Glow Discharge Optical Emission Spectroscopy: A Practical Guide*, Royal Society for Chemistry (2003), https://doi.org/10.1039/9781847550989
15. Z. Weiss, Depth-Resolved Elemental Analysis by Glow Discharge Emission Spectroscopy: Practical Aspects—A Review, *Metals* 2025, 15, 768, https://doi.org/10.3390/met15070768
16. R. Escobar Galindo, E. Forniés, R. Gago, J.M. Albella, Calibration of nitrogen content for GDOES depth profiling of complex nitride coatings, *J. Anal. At. Spectrom*. 22 (2007) 1512–1516, https://doi.org/10.1039/B711657H
17. P. Vlcak, J. Fojt, Z. Weiss, J. Kopeček, V. Perina, The effect of nitrogen saturation on the corrosion behaviour of Ti-35Nb-7Zr-5Ta beta titanium alloy nitrided by ion implantation, *Surf. Coat. Technol.* 358 (2019) 144-152, https://doi.org/10.1016/j.surfcoat.2018.11.004
18. L. Lobo, B. Fernandez, R. Pereiro, N. Bordel, A. Sanz-Medel, Nitrogen effects in multi-matrix calibrations by radiofrequency glow discharge – optical emission spectrometry, *Anal. Bioanal. Chem.* 389 (2007) 743–752, https://doi.org/10.1007/s00216-007-1377-x
19. P. Vlcak, T. Horazdovsky, R. Valenta. J. Kovac, Evolution of the nitrogen depth distribution in an implanted titanium alloy with a surface carbon nanolayer, *Chem. Phys. Lett*. 679 (2017) 25–30, https://doi.org/10.1016/j.cplett.2017.04.066
20. *Manual of the Tecvac 221 ion implanter*, Ver. 1.0, 221-870115
21. Z. Weiss, Calibration methods in glow discharge optical emission spectroscopy: a tutorial review, *J. Anal. At. Spectrom.* 2015, 30, 1038 – 1049, https://doi.org/10.1039/C4JA00482E

22. Z. Weiss, Non-linear intensity response in glow discharge emission spectroscopy. Excitation, radiative transfer and self-absorption, *Spectrochim. Acta Part B* 225 (2025) 107109, https://doi.org/10.1016/j.sab.2024.107109
23. V. Hoffmann, M. Uhlemann, S. Richter, J. Pfeifer, Calibration capacity of hot-pressed hydrogen standards for glow discharge optical emission and mass spectrometry, *Spectrochim. Acta Part B* 176 (2021) 106039, https://doi.org/10.1016/j.sab.2020.106039
24. A. Bengtson, S. Hänström, The influence of hydrogen on emission intensities in GD-OES, consequences for quantitative depth profile analysis, *Proc. of the 5th Intl. Conf. on Progress in Analytical Chemistry in the Steel and Metals Industries (CETAS),* ed. R. Tomellini, European Communities, Luxembourg, 1998, pp. 47–54.
25. Mayer, M. (1997). *SIMNRA User's Guide*. Report IPP 9/113. Max-Planck-Institut für Plasmaphysik, Garching, Germany.
26. E. Rimini, *Ion Implantation: Basics to Device Fabrication*, Springer New York, NY (1995), https://doi.org/10.1007/978-1-4615-2259-1
27. P. Šmíd, E. Steers, Z. Weiss, J. Pickering, V. Hoffmann, The effect of hydrogen and nitrogen on emission spectra of iron and titanium atomic lines in analytical glow discharges, *J. Anal. At. Spectrom.* 2008, 23, 1223–1233, https://doi.org/10.1039/B803812K
28. A. Bogaerts, J. Naylor, M. Hatcher, W.J. Jones, R. Mason, Influence of sticking coefficients on the behavior of sputtered atoms in an argon glow discharge: modelling and comparison with experiment, *J. Vac. Sci. Technol. A* 16 (1998) 2400–2410, https://doi.org/10.1116/1.581359
29. S. Kadlec, J. Musil, and H. Vyskocil, Hysteresis effect in reactive sputtering: a problem of system stability, *J. Phys. D: Appl. Phys.* 19, L187 (1986), https://doi.org/10.1088/0022-3727/19/9/004
30. J. Čapek and S. Kadlec, Return of target material ions: The reason for reduced hysteresis in reactive high power impulse magnetron sputtering – experiment, *J. Appl. Phys*. 121, 171911 (2017). https://doi.org/10.1063/1.4977816
31. W.M. Heuvelman, P. Helderman, G.C.A.M. Janssen, S. Radelaar, TiN reactive sputter deposition studied as a function of the pumping speed, *Thin Solid Films* 332 (1998) 335-339, https://doi.org/10.1016/S0040-6090(98)01203-6
32. J. Musil, M. Jaroš, Š. Kos, R. Čerstvý, S. Haviar, Hard TiN_2 dinitride films prepared by magnetron sputtering, *J. Vac. Sci. Technol. A* 36, 040602 (2018), https://doi.org/10.1116/1.5038555
33. Ph. Belenguer, M. Ganciu, Ph. Guillot, Th. Nelis, Pulsed glow discharges for analytical applications, *Spectrochim. Acta Part B* 64 (2009) 623–641, https://doi.org/10.1016/j.sab.2009.05.031
34. A. Bogaerts, R. Gijbels, R.J. Carman, Collisional-radiative model for the sputtered copper atoms and ions in a direct current argon glow discharge, *Spectrochim. Acta Part B* 53 (1998) 1679–1703, https://doi.org/10.1016/S0584-8547(98)00201-8
35. B. Rauschenbach, K. Hochmuth, Synthesis of compounds by high-fluence nitrogen ion implantation in titanium, *phys. stat. sol. (a)* 94 (1986) 833-837, https://doi.org/10.1002/pssa.2210940251

36. J. Jeans, *An Introduction to the Kinetic Theory of Gases*. Cambridge University Press, 2009. https://doi.org/10.1017/CBO9780511694349

37. N.P. Ferreira, H.G.C. Human, A study of sputtered atoms in the plasma of the modified Grimm-type glow discharge source*, Spectrochim. Acta Part B* 36 (1981) 215–229.

38. A. Revel, A. El Farsy, L. de Poucques, J. Robert, T. Minea. Transition from ballistic to thermalized transport of the metal sputtered species in DC magnetron, *Plasma Sources Sci. Technol.* 30 (2021) 125005, https://doi.org/10.1088/1361-6595/ac352b

39. A. Bogaerts, R. Gijbels, V.V. Serikov, Calculation of gas heating in direct current argon glow discharges, *J. Appl. Phys*. 87 (2000), 8334-8344, https://doi.org/10.1063/1.373545

40. B. Brunetti, G. Liuti, E. Luzzatti, F. Pirani, G.G. Volpi, The interaction of atomic and molecular nitrogen with argon by scattering measurements, *J. Chem. Phys*. 79 (1983) 273–277, https://doi.org/10.1063/1.445576

41. The Engineering Toolbox, [online, 23-03-2026], https://www.engineeringtoolbox.com/air-diffusion-coefficient-gas-mixture-temperature-d_2010.html

42. Z. Weiss, Emission yields and the standard model in glow discharge optical emission spectroscopy: Links to the underlying physics and analytical interpretation of the experimental data, *Spectrochim. Acta Part B* 61 (2006) 121–133, https://doi.org/10.1016/j.sab.2005.11.006

43. V. Hoffmann, B. Gebel, R. Heller, T. Gemming, Investigation of matrix independent calibration of oxygen in glow discharge optical emission spectrometry, *J. Anal. At. Spectrom*. 37 (2022), 1223-1228, https://doi.org/10.1039/d2ja00043a

Analysis of nitrogen implantation profiles in titanium and Ti-Nb alloys by glow discharge optical emission spectroscopy: nitrogen calibration

Z. Weiss, V. Smola, M. Lebeda, P. Vlčák, J. Lorinčík, I. Elantyev, P. Malinský

Data availability statement:

Data for this article, including bitmaps of the Figures and the underlying depth profiles in csv format, are available at Zenodo at https://doi.org/10.5281/zenodo.18493405.